

Supplementary material (ESI) for Journal of Materials Chemistry  
This journal is © The Royal Society of Chemistry 2010

## Supplementary Information

### **Highly efficient visible light sensitized red emission from europium tris[1-(4-biphenoyl)-3-(2-fluoroyl)propanedione](1,10phenanthroline) complex grafted on silica nanoparticles**

**V. Divya, S. Biju, R. Luxmi Varma and M. L. P. Reddy\***

*Chemical Sciences and Technology Division, National Institute for Interdisciplinary Science & Technology (NIIST), CSIR, Thiruvananthapuram-695019, India*

*E mail: [mlpreddy55@gmail.com](mailto:mlpreddy55@gmail.com)*

### Physical Characterization of SiBFPD-Na and Eu<sup>3+</sup> luminescent hexagonal mesoporous silica particles Eu(SiBFPD)<sub>3</sub>(phen)/MCM-41 (**3**)

For the modified ligand SiBFPD-Na a broad peak at  $\delta = 5.12$  ppm in the <sup>1</sup>H NMR (Fig. S6) and  $\delta = 159$  ppm in the solid state <sup>13</sup>C NMR spectra (Fig. S7) indicates the formation of amide –CO–NH linkage. The propyl chain in the ligand gives peaks at 0.57–3.62 ppm in the <sup>1</sup>H NMR and 8.77, 18.63 and 36.79 ppm in the solid state <sup>13</sup>C NMR spectra. The purity of the product was confirmed by the absence of signal at  $\delta = 6.98$  ppm characteristic of the free H in between the two carbonyl groups of HBFPD in the <sup>1</sup>H NMR spectrum. The <sup>29</sup>Si CPMAS NMR spectrum of **3** is shown in Fig. S8. The <sup>29</sup>Si CPMAS NMR spectrum of **3** displays two broad overlapping resonances at  $\delta = -103.59$  and  $-115.01$  ppm, which correspond to Q<sub>3</sub> and Q<sub>4</sub> species of the silica framework [Q<sub>n</sub> = Si(OSi)<sub>n</sub>(OH)<sub>4-n</sub>]. A weak shoulder is also observed at  $\delta = -95.13$  ppm for the Q<sub>2</sub> species. The Q<sub>3</sub> sites are associated with single Si–OH groups that include both free and hydrogen-bonded silanols, and the Q<sub>2</sub> sites correspond to geminal silane diols. Two additional signals appear at  $\delta = -56.9$  and  $-68.16$  ppm, which can be assigned to T<sub>2</sub> and T<sub>3</sub> organosilica species [T<sub>m</sub> = RSi(OSi)<sub>m</sub>(OEt)<sub>3-m</sub>], respectively, indicates that the organic groups are covalently bonded to the silica matrix.<sup>1-3</sup>

The carbonyl stretching frequency of complex **3** has been shifted to lower wave number (1590 cm<sup>-1</sup> of the free ligand, SiBFPD-Na to 1568 cm<sup>-1</sup>), indicating the involvement of carbonyl oxygen in the complex formation with Eu<sup>3+</sup> ion. Further, a red shift observed in the characteristic peak of phen (1561 cm<sup>-1</sup>) in complex **3** (1519 cm<sup>-1</sup>), shows the involvement of nitrogen in the complex formation with Eu<sup>3+</sup> ion.<sup>4</sup> The FT-IR spectra of the grafted ligand SiBFPD-Na and complex **3** are shown in Fig. S4. The presence of the amide group in SiBFPD-Na was confirmed by the appearance of new bands at 3335 ( $\nu$  NH), 1629 cm<sup>-1</sup> ( $\nu$  NHCO) and 1443 cm<sup>-1</sup> ( $\delta$  NH). Three peaks at 2961, 2923 and 2851 cm<sup>-1</sup> are related to C–H stretching of sp<sup>3</sup> carbon. An intense band at 1076 cm<sup>-1</sup> can be observed and is assigned to an asymmetric stretching of siloxane groups.<sup>5</sup> The FT-IR spectrum of complex **3** consists of a broad band located at around 1083 cm<sup>-1</sup> ( $\nu_{as}$ , Si—O), 847 cm<sup>-1</sup> ( $\phi$ , Si—O), and 548 cm<sup>-1</sup> ( $\delta$ , Si—O—Si), which attributes to the success of hydrolysis and copolycondensation reactions ( $\nu$  represents stretching,  $\delta$  in plane bending,  $\phi$  ring deformation, s symmetric, and as asymmetric vibrations).<sup>2</sup> The

band at  $960\text{ cm}^{-1}$  can be assigned to stretching vibrations of Si—OH surface groups. The peak at  $1629\text{ cm}^{-1}$  originating from the —CONH— group of SiBFPD-Na, can also be observed in **3** which is consistent with the fact that the carbonyl group of the precursor remain invariably after hydrolysis and condensation reactions, confirming that the two carbonyl groups of  $\beta$ -diketones are coordinated to the  $\text{Eu}^{3+}$  ions, not the carbonyl group of the TESPIC.<sup>2,3</sup>

The FT-Raman spectra of the SiBFPD-Na ligand and complex **3** are shown in Fig. S5. The peak at  $1404\text{ cm}^{-1}$  in the ligand and at  $1421\text{ cm}^{-1}$  in **3** are due to the symmetric stretching vibrations of the C=O group ( $\nu_{\text{s}}\text{C=O}$ ). The peak at  $1606\text{ cm}^{-1}$  originating from the —CONH— group of SiBFPD-Na, remains as the same in the complex **3** proves that carbonyl group of the TESPIC is not involved in the coordination with metal ions.<sup>2</sup> The peaks at around  $1384\text{ cm}^{-1}$  in both the ligand and in **3** are due to the in-plane bending of  $\text{CH}_2$  group ( $\delta\text{CH}_2$ ). In the vibrational spectrum of **3**, band arising from the ancillary ligand phen was observed at  $1520\text{ cm}^{-1}$ ,<sup>4</sup> indicating the presence of phen in **3**. The detailed vibrational spectral data are given in Table S1.

From the dynamic light scattering (DLS) measurements it is evident that the mesoporous hybrid material has an average particle size of 364 nm (Fig. S9). Scanning electron microscopy (SEM) picture of the mesoporous hybrid material is given in Fig. S10. The SEM picture of mesoporous hybrid material is typical for the covalently bonded hybrids with mesoporous host and show the morphology of aggregated spherical particles of diameter of around 100-300 nm. Meanwhile, the different tendency of the polycondensation reaction of Si—O—Si in the three dimensions caused the different sizes in length and in width.<sup>6a</sup> The morphology and size of the grafted nanoparticles were examined by TEM analysis (Fig. S11). The picture indicate that the monodispersity of the nanosized MCM-41 units was conserved in the mesoporous hybrid material.<sup>2,6b</sup>

The X-ray diffraction (XRD) patterns are popular and efficient method to characterize highly ordered mesoporous materials with hexagonal symmetry. The XRD pattern for MCM-41 is characteristic of three well-defined Bragg peaks in the low angle range corresponded to the d (100), (110), and (200) planes of the solid that are fully indexed to a hexagonal unit cell (Fig. S12). In addition to the d (100) peak, a broad diffraction peak was noted in the low  $2\theta$  region at 3.27 in **3**, which is a characteristic peak of the

formation of periodic hexagonal mesostructures.<sup>5a,7a-b</sup> The broadening of peaks also reveals that the structure ordering decreases with the anchoring of **2**. This result also provides indirect evidence that complex **3** is indeed incorporated into the mesoporous silica framework. The presence of d (100) peak suggested that the framework stability was still maintained for the grafted complex.<sup>7c</sup>

Nitrogen adsorption-desorption isotherms obtained for the complex **3** shows that the reduction of the surface area from  $731\text{ m}^2\text{ g}^{-1}$  for the MCM-41 to  $11\text{ m}^2\text{ g}^{-1}$ , suggesting that micro-environment of MCM-41 has drastically changed due to the introduction of luminescent centers on the pore surface. Likewise, the pore volume for MCM-41 for  $0.73\text{ cm}^3\text{ g}^{-1}$  decreased to  $0.02\text{ cm}^3\text{ g}^{-1}$  which might be due to the fact that the presence of bulky organic ligand on the pore surface interact with surfactant reduce the pore volume. This loss in surface area may be explained by the fact that  $\text{N}_2$  molecules are repelled from the silica surface by the grafted organosilanes so that they cannot adsorb any more.<sup>2,8</sup>

The thermal behavior of the complex **3** was examined by means of thermogravimetric analysis (TGA) under nitrogen atmosphere and the results are depicted in the Fig. S3. Complex **3** showed two distinct stages of decomposition. The first weight loss around  $100\text{ }^\circ\text{C}$  as related to absorbed water and the other one between  $100\text{-}600\text{ }^\circ\text{C}$  was assigned to the decomposition of organic matter and water from silyl group condensation.<sup>5a</sup> In addition, compared with the weight loss at  $600\text{ }^\circ\text{C}$  ( $\sim 68\text{ %}$ ) of pure complex **2**, the decomposition of **3** was lower ( $\sim 38\text{ %}$ ), indicating that the thermal stability of the pure complex was enhanced as it was covalently bonded to the mesoporous matrix.

## References

- 1 S. M. Bruno, A. C. Coelho, R. A. S. Ferreira, L. D. Carlos, M. Pillinger, A. A. Valente, P. Ribeiro-Claro and I. S. Goncalves, *Eur. J. Inorg. Chem.*, 2008, 3786.
- 2 D. B. Ambili Raj, S. Biju and M. L. P. Reddy, *J. Mater. Chem.*, 2009, **19**, 7976.
- 3 (a) X.-F. Qiao and B. Yan, *Inorg. Chem.*, 2009, **48**, 4714; (b) X. Qiao and B. Yan, *J. Phys. Chem. B*, 2008, **112**, 14742.
- 4 L.-J. Bian, H. Xi, X.-F. Quan, J. Yin, Z.-K. Zhu and Q.-H. Lu, *Mater. Res. Bull.*, 2002, **37**, 2293.

- 5 (a) E. De Oliveira, C. R. Neri, O. A. Serra and A. G. S. Prado, *Chem. Mater.*, 2007, **19**, 5437; (b) P. T. Tanav and T. J. Pinnavaia, *Chem. Mater.*, 1996, **8**, 2068.
- 6 (a) J. L. Liu and B. Yan, *J. Phys. Chem. B*, 2008, **112**, 10898; (b) S. Cousinié, M. Gressier, C. Reber, J. Dexpert-Ghys and M.-J. Menu, *Langmuir*, 2008, **24**, 6208.
- 7 (a) Y. Li, B. Yan and H. Yang, *J. Phys. Chem. C*, 2008, **112**, 3959; (b) M. Ogawa, K. Ikeue and M. Anpo, *Chem. Mater.*, 2001, **13**, 2900; (c) Y.-S. Lin, Y. Hung, J.-K. Su, R. Lee, C. Chang, M.-L. Lin and C. Y. Mou, *J. Phys. Chem. B*, 2004, **108**, 15608.
- 8 (a) B. Yan and B. Zhou, *J. Photochem. Photobiol. A*, 2008, **195**, 314; (b) S. Cousinié, M. Gressier, C. Reber, J. Dexpert-Ghys and M.-J. Menu, *Langmuir*, 2008, **24**, 6208.

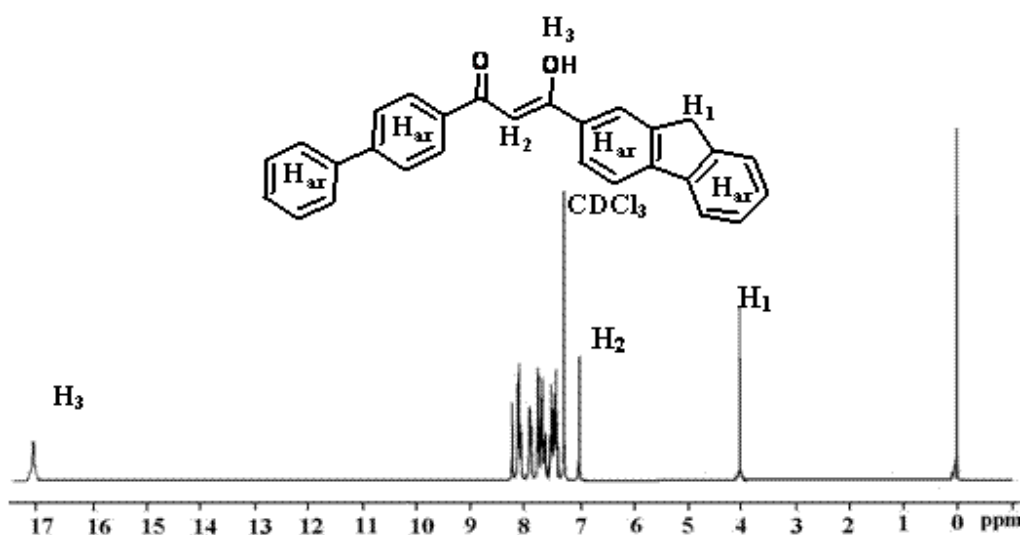


**Fig. S1.** <sup>1</sup>H NMR spectrum of the ligand HBFPD.

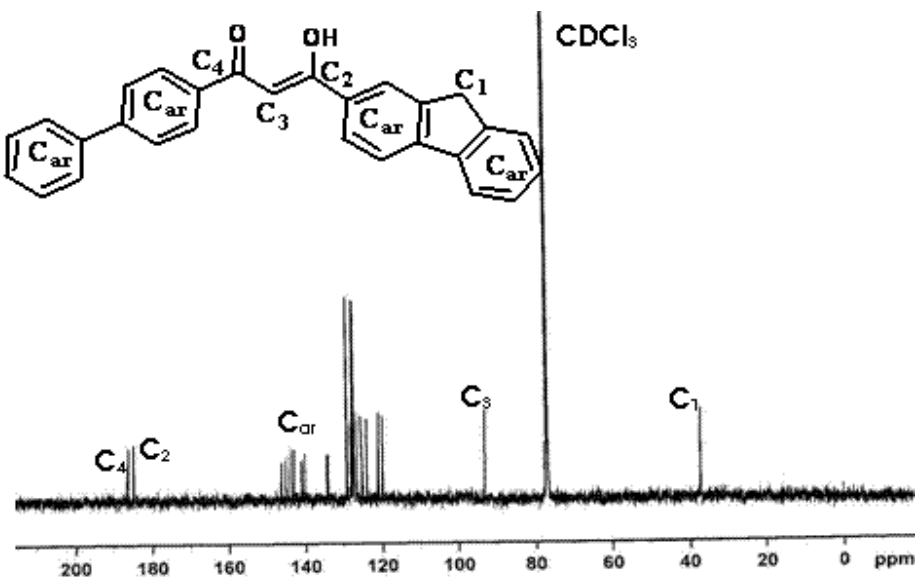


**Fig. S2** <sup>13</sup>C NMR spectrum of the ligand HBFPD.

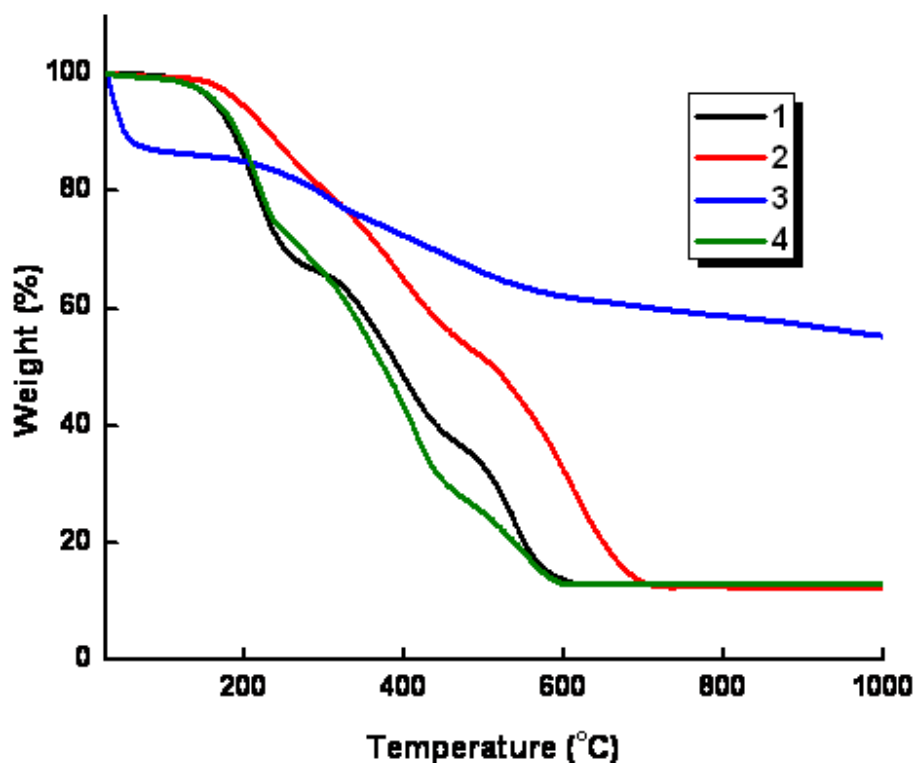


**Fig. S3** Thermogravimetric curves for the complexes 1-4.

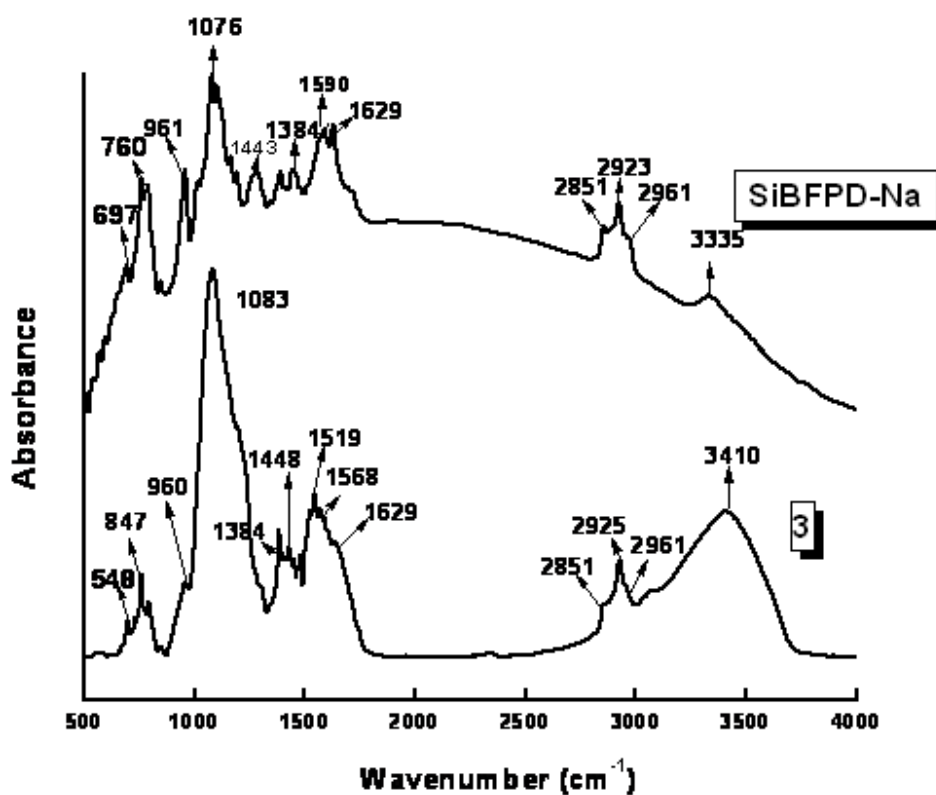


**Fig. S4** FT-IR spectra of the ligand SiBFPD-Na and complex **3**.

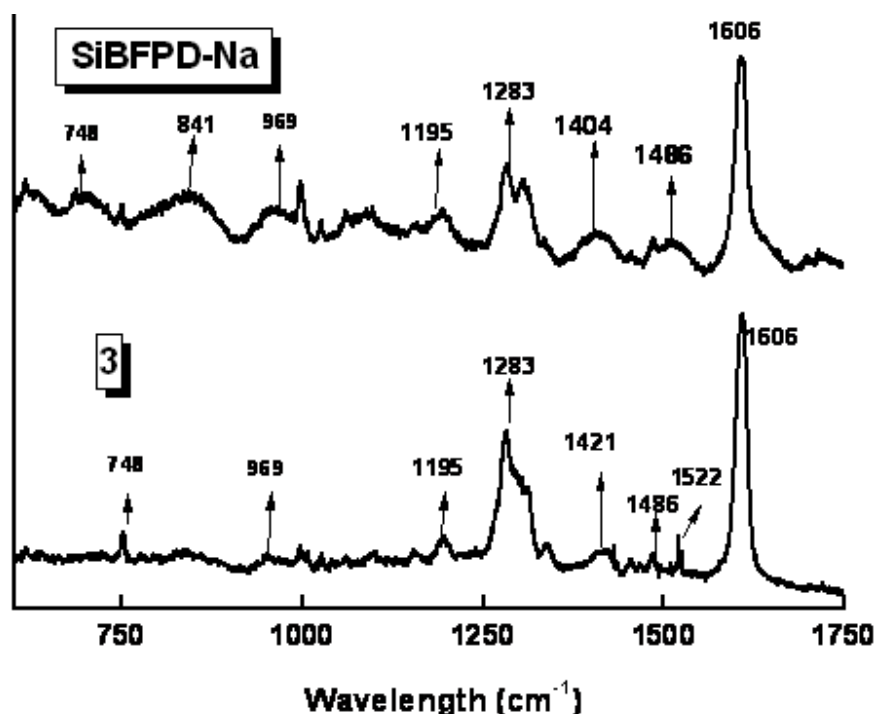


**Fig. S5** FT-Raman spectra of the ligand SiBFPD-Na and complex 3.

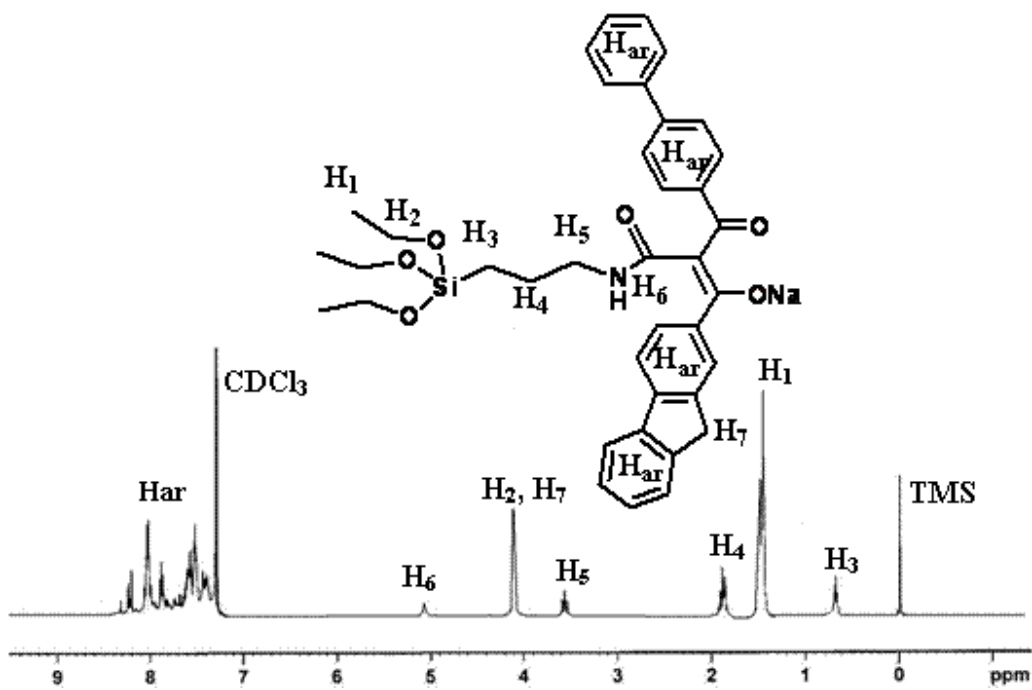


**Fig. S6** <sup>1</sup>H NMR spectrum of the ligand SiBFPD-Na.

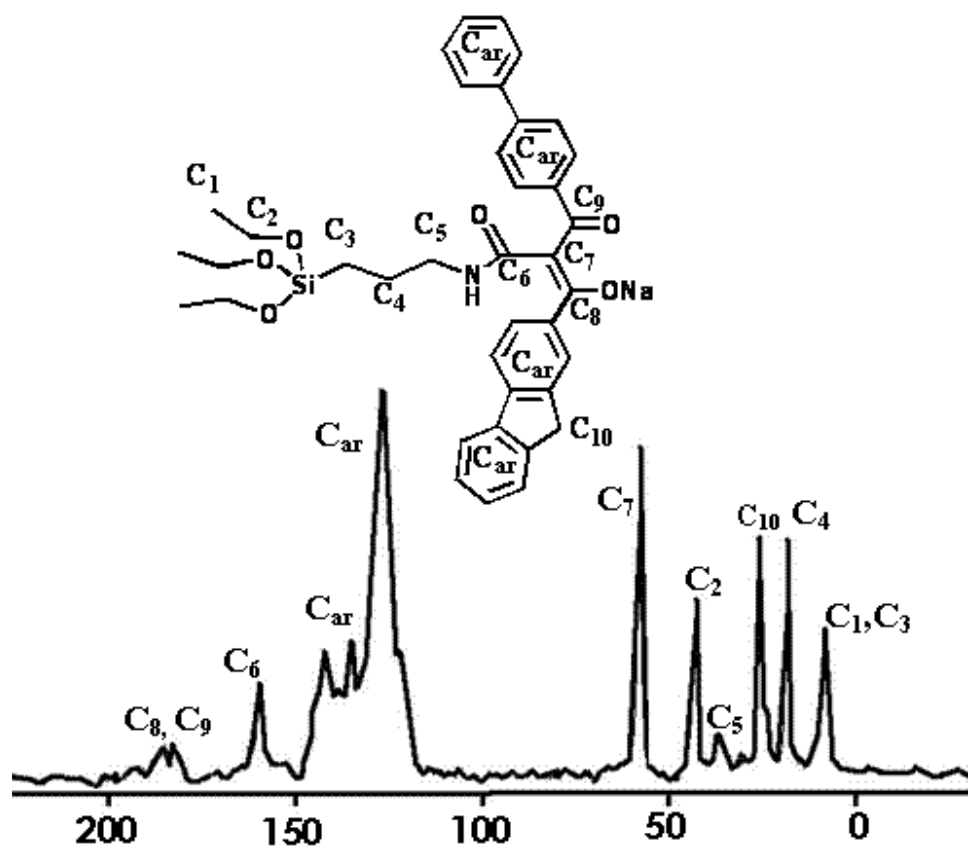


**Fig. S7** Solid state  $^{13}\text{C}$  NMR spectrum of the ligand SiBFPD-Na.

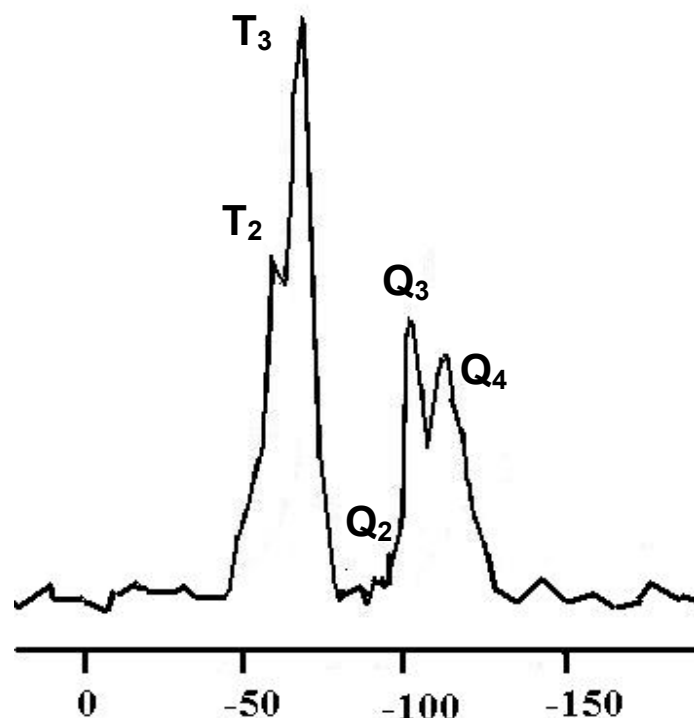


**Fig. S8** Solid state  $^{29}\text{Si}$  CPMAS NMR spectrum of complex 3.

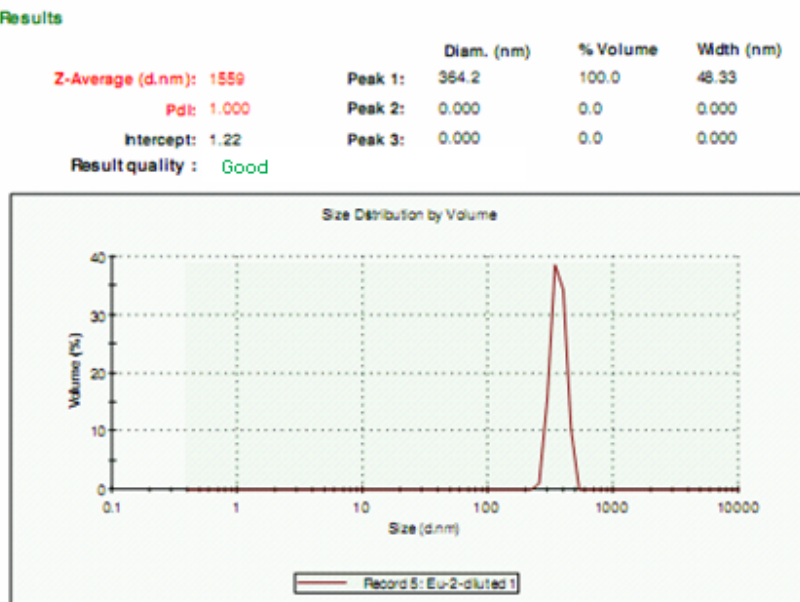


**Fig. S9** DLS particle size distribution curve for **3**.

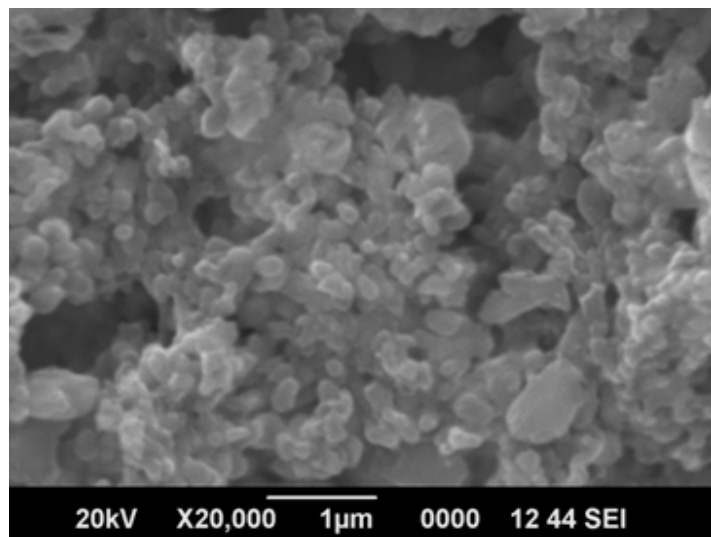


**Fig. S10** SEM micrograph of the complex **3**.

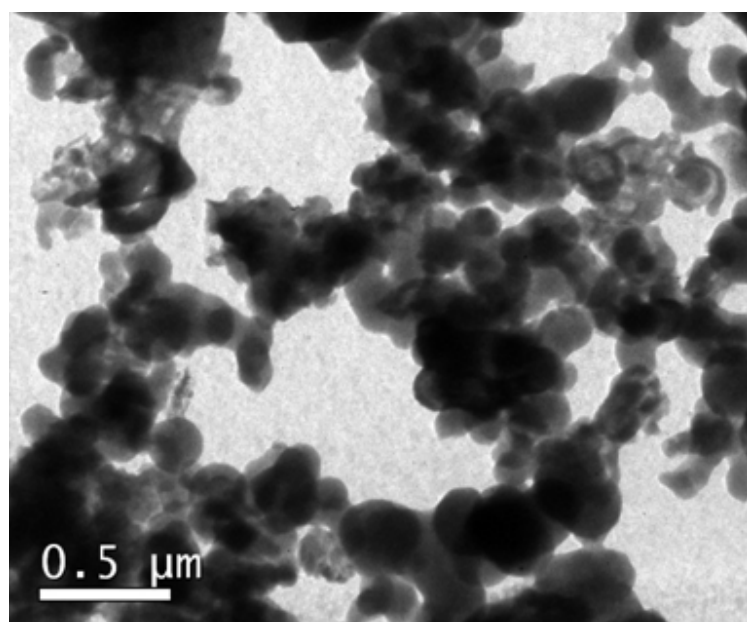


**Fig. S11** TEM micrograph of the complex **3**.

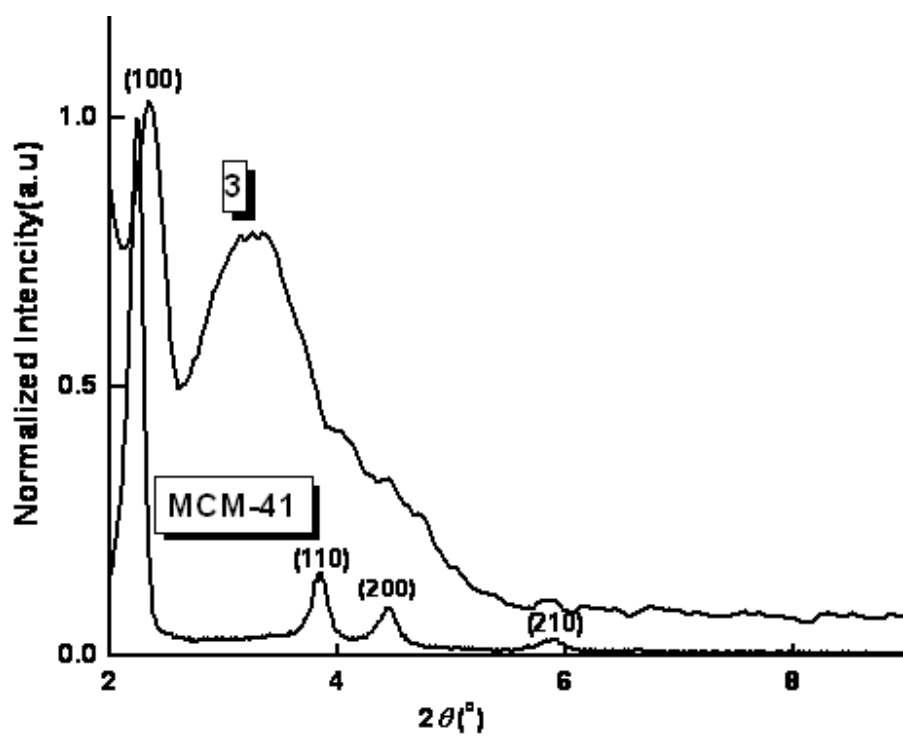


**Fig. S12** Powder XRD patterns of MCM-41 and complex **3**.

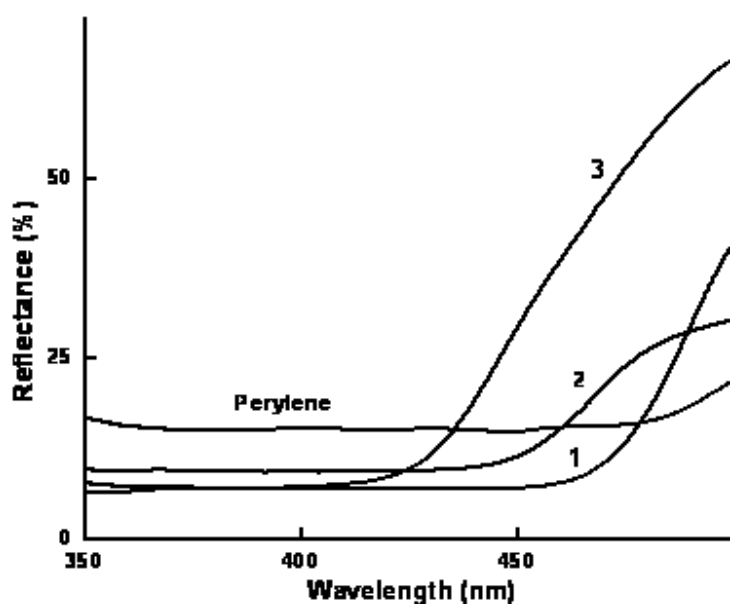


**Fig. S13.** Diffuse reflectance spectra of complexes **1-3** and the standard phosphor perylene.

**Table S1** Wavenumbers observed in FT-IR and FT-Raman Spectra of the samples and the respective vibrational assignments for the silylated ligand SiBFPD-Na and complex **3**

| SiBFPD-Na |       | <b>3</b> |       | description                            |
|-----------|-------|----------|-------|--|
| IR        | Raman | IR       | Raman |  |
| 3335      | —     | 3410     | —     | $\nu(\text{N-H})$                      |
| 1629      | 1606  | 1629     | 1606  | $\nu(\text{NHC=O})$                    |
| 1443      | —     | 1448     | —     | $\delta(\text{N-H})$                   |
| 1590      | 1404  | 1568     | 1421  | $\nu_s(\text{C=O})$                    |
| 2923      | —     | 2925     | —     | $\nu(\text{C}_{\text{SP}}^3\text{-H})$ |
| 2961      | —     | 2961     | —     | $\nu(\text{C}_{\text{SP}}^3\text{-H})$ |
| 2851      | —     | 2851     | —     | $\nu(\text{C}_{\text{SP}}^3\text{-H})$ |
| —         | 1284  | —        | 1283  | $\phi_v(\text{C-C})$                   |
| 1384      | 1384  | —        | 1384  | $\delta(\text{CH}_2)$                  |
| —         | —     | 1519     | —     | $\nu(\text{C=N})$                      |
| —         | 1486  | —        | 1486  | $\nu(\text{C=C})$                      |
| 1076      | 1195  | 1083     | 1195  | $\nu_{as}(\text{Si-O})$                |
| —         | 748   | 847      | 748   | $\phi(\text{Si-O-Si})$                 |
| —         | —     | 548      | —     | $\delta(\text{Si-O-Si})$               |
| 961       | 969   | 960      | 969   | $\nu(\text{Si-OH})$                    |